



Gravel bar shielding: A mechanism responsible for bar stability in gravel- and cobble-bedded streams

Ariel do Prado¹  | Cristiano Padalino Galeazzi² | David Mair¹  |
 Philippos Garefalakis¹ | Renato Paes de Almeida³ | Alexander C. Whittaker⁴ |
 Fritz Schlunegger¹

¹University of Bern, Institute of Geological Sciences, Bern, Switzerland

²School of Earth and Environmental Sciences, Seoul National University, Seoul, Republic of Korea

³Instituto de Geociências, Universidade de São Paulo, São Paulo, Brazil

⁴Department of Earth Science and Engineering, Imperial College, London, UK

Correspondence

Ariel Henrique do Prado, University of Bern, Institute of Geological Sciences, Baltzerstrasse 1+3, 3012 Bern, Switzerland.
 Email: ariel.doprado@unibe.ch

Funding information

European Union's Horizon 2020, Grant/Award Number: 860383; National Research Foundation of Korea, Grant/Award Numbers: RS-2022-NR070842, RS-2023-00301976

Abstract

The stability of gravel bars and riverbanks is often attributed to the presence of vegetation, yet the conditions controlling the stability of such bars without of a vegetation cover have remained unclear. Here, we propose that such controls are exerted by what we refer to as 'lateral lag deposits', which result from the winnowing of gravel bar edges during periods when channels widen. We base this interpretation on an example from the Sense River, Switzerland, a natural wandering-braided stream with gravel-cobble bars devoid of vegetation. Through a survey where we measured the size of several thousands of grains along two up to 50 m-long reaches, we found that the 84th percentile values (D_{84}) of the grain size distributions (GSD) are consistently larger on the eroded bar edges compared to the bar top or the channel between bars. At these bar edges, the coarse grains appear to shield the gravel bar from lateral erosion, thus forming a lag deposit. Orthoimages taken along the studied reaches between 2017 and 2023 reveal that the target lateral lag deposits outlasted several lower-discharge floods, during which the sedimentological architecture of the investigated reach changed multiple times. We therefore suggest that lateral lag deposits are among the sedimentological structures of braided streams with the highest preservation potential and that they exert the largest threshold to the complete reworking of gravel bars without vegetation.

KEYWORDS

bar stability, grain size, gravel bar, sediment transport

1 | INTRODUCTION

Assessing the processes responsible for the formation of gravel bars in streams is key for understanding the geomorphology of coarse-grained rivers (Bridge, 2003; Church & Jones, 1982; Reid et al., 2019). A quantitative evaluation of the characteristics of such bars, such as roughness, grain size, slope and their variations along a reach, provides valuable insights into the conditions and processes that influence the stability of channels and control the transport of sedimentary material (e.g. Mao, Dell'Agnese, & Comiti, 2017; Recking et al., 2008). The results of such a quantitative evaluation also offer proxy

information for estimating the effectiveness of flood events to mobilize bedload material (Wolman & Gerson, 1978), which is crucial knowledge for restoration and management practices (Doyle et al., 2007). Neglecting the mechanisms that result in the stability of a gravel bar can therefore lead to inaccurate models about the relationships between flood magnitudes and sediment transport, such as bedload.

Changes in riverbed morphology occur during flood (or bankfull-flow) stages when a significant portion of the available material on the riverbed is transported (Ashmore, 2013; Eaton, MacKenzie, & Booker, 2020; Galeazzi, Almeida, & Do Prado, 2021; Sambrook Smith

This is an open access article under the terms of the [Creative Commons Attribution-NonCommercial-NoDerivs](https://creativecommons.org/licenses/by-nc-nd/4.0/) License, which permits use and distribution in any medium, provided the original work is properly cited, the use is non-commercial and no modifications or adaptations are made.

© 2025 The Author(s). *Earth Surface Processes and Landforms* published by John Wiley & Sons Ltd.

et al., 2010). During such floods, river bars can be completely modified, yet some of them also remain stable. It has been proposed that the presence of vegetation on these bars exerts a large control on their stability, where the roots protect the bar material from being entrained (Anderson, Bledsoe, & Hession, 2004; Eaton, 2006; Jourdain et al., 2020). For bars without vegetation, however, the stability is controlled by threshold stresses, conditioning the entrainment of clasts (e.g. Reid et al., 2019). When such thresholds are exceeded, the coarsest grains on a bar surface may be entrained, with the result that not only the morphology of the associated gravel bar but also that of the adjacent channel begins to change (Church, 2006; MacKenzie & Eaton, 2017). These stresses can be divided into bed shear stress and bank shear stress, both of which influence the width and depth of a channel. These factors are controlled by various elements, including the geometries of the riverbed and bank, frictional forces, energy gradient (i.e., channel slope), water depth and other hydraulic conditions (e.g. Millar & Quick, 1993; Parker, 1978). However, spatial variations in the grain size distribution (GSD) of a bar consisting of patches (do Prado et al., 2025; Nelson et al., 2009) with different roughness and friction properties (e.g., Aberle & Smart, 2003) complicate applications of simple relationships between water flow, shear stress and material entrainment. Besides water depth and channel slope, the flow's shear stress is also influenced by turbulent interactions between the fluid (in this case water) and the sedimentary material along the channel edges, making predictions about the motion of bedload material even more complicated (Eaton, MacKenzie, & Booker, 2020; Pizzuto, 1990). This is particularly the case for bar edges composed of coarse-grained material, for which the mechanisms and conditions during the incipient motion of clasts have been an overlooked topic. Yet, research on this aspect is important because bar edges have the potential to protect the entire bar from being eroded, thereby maintaining the channel in a stable position.

In this work, we document the occurrence of bar edges composed of coarse-grained material, which we term “lateral lag deposits”. We also propose a conceptual model of how they form and explore their role in controlling the stability of a network of channels and bars. We proceed by describing, as a first step, the morphology of three studied gravel bars observed in a natural stream in Switzerland, where we measured the sizes of grains and determined the pattern of surface roughness. We show that such bar edges consist of sediment that is coarser-grained and exerts a larger roughness on the flowing water than the material on the top of the same bar and along the bordering channel. We also document that they tend to stabilise the ensemble of channels and bars. We suggest that this newly recognized structure should be considered alongside other bedforms that develop under low sediment supply conditions in gravel-bedded rivers, such as pebble clusters, stone lines and riffles, all of which contribute to stabilizing the channel's longitudinal profile (Montgomery & Buffington, 1997; Venditti et al., 2017).

2 | LOCAL SETTING

The Sense River, which is the target stream for this study, is a perennial river with a wandering-braided gravel pattern located at the northern margin of the Swiss Alps (Figure 1 and Figure A1 in the Supporting Information). It originates from the confluence

between the Kalte and Warme Sense tributaries, encompassing a drainage area of about 435 km². The bedrock of the upstream catchment is made up of strongly folded alternations of Mesozoic limestone beds and marls that are exposed in the Penninic Klippen belt, and thrust and folded Late Cretaceous to Early Tertiary sandstone-mudstone suites referred to as the Gurnigel Flysch (Tercier & Bieri, 1961; Tonolla, Geilhausen, & Doering, 2021). The Sense River itself has been described as one of the most pristine rivers within the northern Alpine region (Hettrich et al., 2011). Two sites along the river are investigated in this study (see Figure 1). The first one, referred to as Site A (46.749813°, 7.304307°; WGS 84), is located in an unconfined multi-thread reach of the Sense River, encompassing a drainage area of about 125 km². The second one is referred to as Site B (46.717750°, 7.309347°; WGS 84) and is situated in a confined single-channel reach of the Kalte Sense River about 5 km farther upstream of Site A near to the confluence with the Warme Sense River. The corresponding drainage area of Site B measures about 46 km². During reconnaissance work, we observed multiple bedforms that we interpret as lateral lag deposits in the reaches surrounding both study sites, typically bordering active and, in some cases, inactive channels. The occurrence of such lateral lag deposits is the main reason why we selected these two sites for our survey. In addition, the geomorphic condition where multiple bedforms are present allowed for the measurement of grain sizes and the comparison of the resulting grain size distributions and roughness values across key bedforms features, such as abandoned channels, bar edges and bar tops.

A mean annual discharge of 8.5 m³ s⁻¹ and slope of about 0.01 m m⁻¹ was measured at the ‘Thörishaus-Sensematt’ hydrological station (size of drainage area is 349 km²), located about 20 km downstream of Site A (FOEN, 2024). In addition, for the Thörishaus-Sensematt site, the estimated annual peak discharge values with return periods of 2 years, 10 years, and 100 years are: 143 m³ s⁻¹, 240 m³ s⁻¹ and 402 m³ s⁻¹, respectively (Figure A2 in the Supporting Information; FOEN, 2024). Peak discharge events are driven by periods of intense precipitation, which occur most frequently during the summer but can also happen throughout the year. Along the studied reaches, the bedload regime has been considered to be in a near-equilibrium state, with an estimated annual bedload supply from the Kalte and Warme Sense tributaries of about 7,500 m³ (GEKOB, 2014).

3 | METHODS

We collected grain size data using the workflow that is outlined in do Prado et al. (2024, 2025) and summarized below. Accordingly, we took digital images with an uncrewed aerial vehicle (UAV) and processed them using state-of-the-art photogrammetric methods (See details in section 3.1). We used the results of the UAV survey to generate digital elevation models (DEMs) and orthomosaics with a spatial resolution of about 2 mm pixel⁻¹. Using these orthoimages and DEMs, we mapped the morphological features such as the top and the edge of the target gravel bar and the channel in between them. We then applied a grid-by-number method to measure the sizes of grains within each of these features (See details in Section 3.2). We also calculated the surface roughness along the gravel bars using the

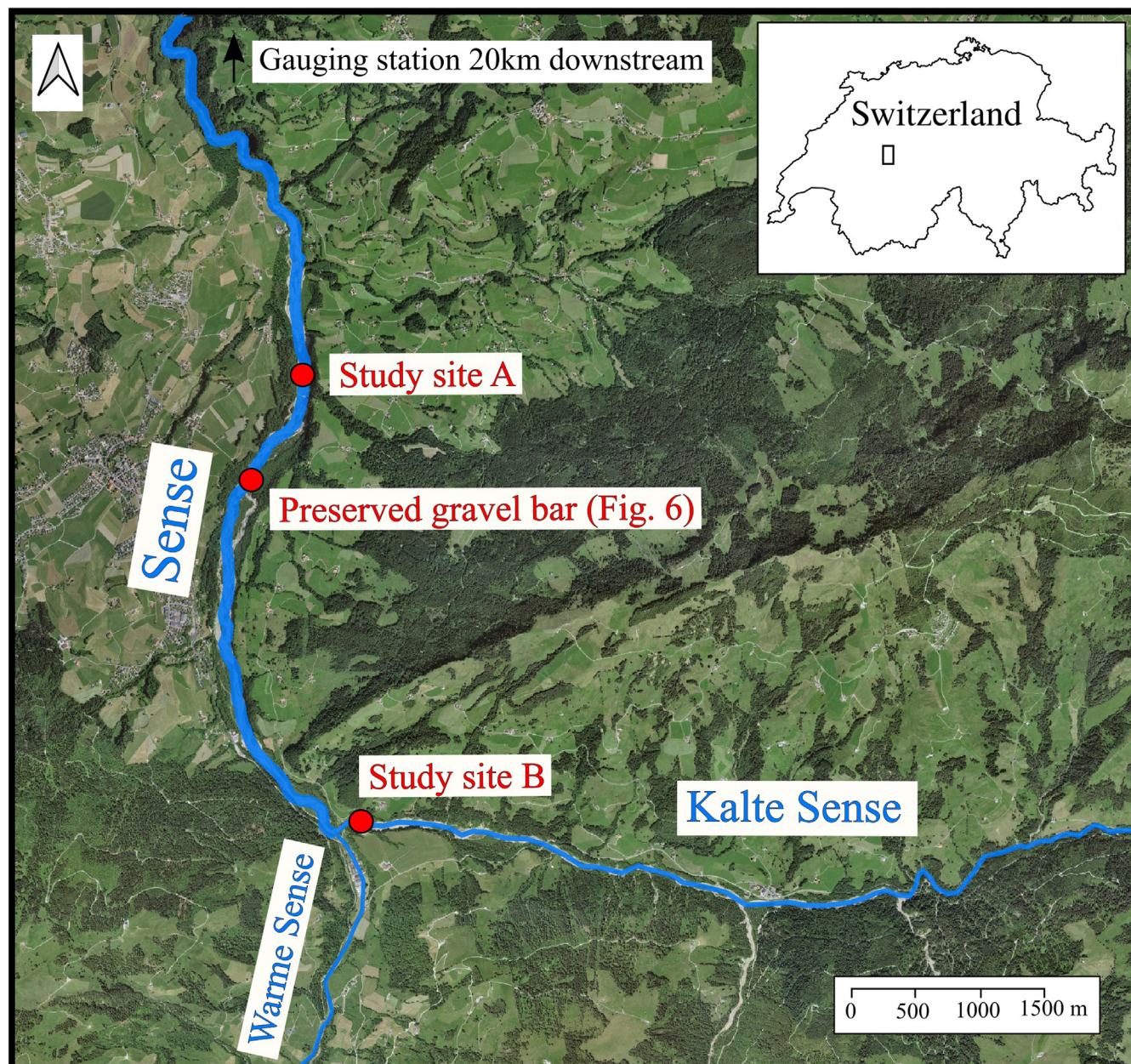


FIGURE 1 Aerial orthoimage of the Sense river (© swisstopo, 2024; Mapgeo, 2024) with the location of the studied sites.

DEMs as input data (See details in section 3.3). This enabled the production of maps showing the spatial variation in surface roughness across the entire study area, providing complementary data to the grain size data, which was specifically collected within each of the mapped bedforms.

3.1 | Uncrewed aerial vehicle (UAV) surveys and photogrammetry processing

Similarly to do Prado et al. (2024, 2025), we applied a UAV close-range setup between October and December 2021 to gravel bars that emerged along the Sense and the Kalte Sense reaches. The goal was to obtain high-resolution DEMs and to measure the distribution of grain sizes (GSDs). The subsequent photogrammetric processing was accomplished following the protocol in Mair et al. (2022). This approach was chosen to mitigate the uncertainties that are inherently

associated with field surveys and the subsequent determination of the size of grains. To ensure a sufficient ground sampling distance of $< 2 \text{ mm pixel}^{-1}$ in all pictures, we conducted the close-range surveys with a flight altitude between 6.64 and 7.34 m above ground. For image acquisition, we used a one-level grid of nadir camera positions as a backbone geometry, for which we targeted 80% of lateral and frontal overlap between individual images. We complemented this grid with images (about 50) taken with oblique angles (pitch of $> 20^\circ$). The images were taken at the same survey altitude to minimize systematic errors during the photogrammetric processing (Carboneau & Dietrich, 2017; James et al., 2020; James & Robson, 2014). All images were taken in the JPEG format with a DJI Mavic 2 Pro on-board camera (Hasselblad L1D-20c), which utilises a global shutter. For referencing, we distributed ground control points (GCPs) over each target gravel bar and measured them with a Leica Zeno GG04 Plus GNSS antenna that allows for a real-time online correction (Swipos-GIS/GEO RTK). This setup yields a horizontal and vertical

precision of 2 cm and 4 cm (2σ), respectively, under ideal conditions (swipos, 2024). The subsequent photogrammetric processing followed standard Structure-from-Motion (SfM) workflows (e.g., Eltner et al., 2016; Fonstad et al., 2013; James & Robson, 2012) including recent updates (e.g., James et al., 2020) to produce high-quality orthomosaic and digital surface models (DSMs) for each gravel bar (Figures 3 and 4).

To generate the DSMs we used the Agisoft Metashape (v1.6 Pro) software, licensed to the Institute of Geological Sciences, University of Bern. This generation consistently involved (i) the manual removal of blurred images, (ii) the use of 'highest-quality' settings in the Metashape for initial image alignment and (iii) subsequent filtering of the tie point clouds (see Mair et al., 2022). The GCPs were used for georeferencing and standard camera modelling. In total, we processed 2 SfM models, with an average checkpoint/GCP georeferencing accuracy of 14 ± 7 mm and systematic errors < 2 cm (Table A1). The DSMs included vegetation, wood debris and water bodies, which we clipped to generate the DEMs, thereby displaying only the ground elevation.

3.2 | Mapping of bed features, and measuring the size of grains

In terms of mapping, we categorized the morphology of the target reaches as bar top, bar edge and channel (Figure 2). We defined the bar edge as the area between two breaks-in-slope, with the slope direction perpendicular to the water flow (e.g., Hassan, 2005). Accordingly, the part of the bar above the edge is the bar top, whereas the area below the bar edge is referred to as the channel. This can either be an abandoned channel or a channel that is active during flood stages only.

For the three geomorphic elements we manually measured the size of grains in a GIS environment offered by the open-source software QGIS (version 3.28; QGIS, 2024). We created a grid on the orthomosaics resulting from the field surveys (see section above), on which we measured the size of grains using a grid-by-number approach (e.g. Church, 1987; Ibbeken & Schleyer, 1986; Rice & Church, 1996; Wolman, 1954). To prevent double counting of particles, the grid spacing is typically determined by the size of the coarsest grain in the measurement area (e.g. Bunte & Abt, 2001). For simplicity, we uniformly set the grid spacing at 0.5 m for both sites, given that the fraction of grains exceeding 0.5 m is consistently below 0.5%. For each grain underneath a grid intersection, we measured the lengths of the a - and b -axes (i.e., the longest and intermediate grain axes, respectively). This was accomplished by fixing four dots at the grains' edges

(e.g. do Prado et al., 2024; Garefalakis et al., 2023), thereby using these to define the two perpendicular axes. Note that in the results section, we present the lengths of the b -axis only as this is commonly employed in equations computing bedload transport (e.g. Recking et al., 2008). Note also that coarser grains appearing at multiple grid intersections were measured only once. Considering the resolution of the images (Table A1 in the Supporting Information) we defined a threshold of 20 mm for the size of a grain to be measured. Accordingly, all grains smaller than this threshold were considered equal to 20 mm. The results show that this consideration did not affect our values of the 50th or 84th grain size percentiles of the resulting GSDs since the proportion of grains smaller than 20 mm was never larger than 25%. We then calculated the 50th, 84th and 96th percentile values (i.e., the D_{50} , D_{84} and D_{96}) from the grain size dataset to characterise the GSDs of the studied sites. These percentiles are commonly used as reference values when assessing the thresholds for riverbed erosion and sediment entrainment (e.g., MacKenzie, Eaton, & Church, 2018; Shields, 1936). We estimated the uncertainties on the grain size datasets through bootstrapping.

3.3 | Detrending DEMs from bedform roughness and parametrizing of roughness variations across space

The pixel sizes of the target DSMs (section 3.1) range between 3 and 4 mm, and all vegetation and woody debris were manually removed to create digital elevation models (DEMs) of the gravel bars. We applied a filter to the DEMs to remove effects related to the roughness exerted by individual grains on the bedforms (grain-scale roughness; Bertin, Groom, & Friedrich, 2017). We proceeded following the method presented by Smart, Duncan, & Walsh (2002) and applied by Bertin, Groom, & Friedrich (2017). Accordingly, a trend surface was fitted to a regular grid with a point spacing equal to 1.25 multiplied by the value of the D_{90} measured in the DEM area. The elevations of grid points were determined by averaging DEM data points within a circle that has a diameter $2.5 \times D_{90}$, centred on each grid intersection. A bi-cubic spline interpolation was then applied to interpolate between the grid points (i.e., locations of the measured DEM points) defining the trend surface. The subtraction of the interpolated trend surface from the original DEM is expected to eliminate larger-scale undulations (humps and hollows) that exceed the size of particle clusters. Our calculations were implemented with functions that are implemented in the QGIS open-source software (QGIS, 2024).

We analysed how the roughness spatially changes upon moving a 2×2 m square window across our DEMs following Groom, Bertin, & Friedrich (2018). We proceeded through investigating how the surface elevation varies around the mean (σ_z) by:

$$\sigma_z^2 = \frac{1}{N} \sum_{i=1}^N (Z_i - \mu)^2, \quad (1)$$

where N is the total number of elevation points in the DEM window, Z_i is the elevation point value at a specific coordinate and μ is the mean elevation in the window. This approach can be used for parametrizing the grain-roughness values in equations of flow resistance (Aberle & Smart, 2003; Noss & Lorke, 2016).

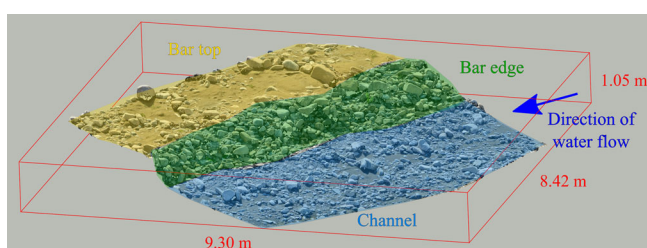


FIGURE 2 3D visualization of the mapped bed features at site A. The area depicted in this image is shown in Figure 3b.

4 | RESULTS

4.1 | Bar morphology

At Site A (Figure 3a), the interpreted “channel” is about 20 m wide and has a mean slope of about 0.01 m m^{-1} (blue area on Figure 3b). It is bordered by gravel bars with heights of about 1 m on both sides. Note that we consider this part of the area as an inactive channel because it has a lower elevation than the bordering bars, and it is relatively flat. Note also that during the time of data acquisition, this inactive channel is part of a gravel bar at a larger scale (Figure 3a), but it takes the function of a channel during flood events. This is particularly visible by the scour marks which are aligned parallel to the channel's border (red lines in Figure 3c and blue arrows in Figure 3d). The gravel bars bordering the channel on

either side have relatively steep edges (about 0.1 m m^{-1}) that are up to 5 m wide and 40 m long (Figure 3b, areas with green and yellow colours). The borders of the edges display distinct break-in-slopes between the channel and the bar top. The bars themselves have similar slopes as the channel. In the survey area, the top surfaces are generally smooth, but some bumps are also visible in places. In addition, the bar top hosts patches with sand that are randomly distributed on the surface.

Along Site B, the ensemble of channel, bar edges and tops are also preserved (Figure 4) and they share nearly the same morphometric properties as those along the Sense reach. The only difference concerns the width of the channel, which is 10 m wide along Site B, making it narrower (half the width) compared to Site A. Note that at both sites, no vegetation has been developed either along the channel or on the bar tops.

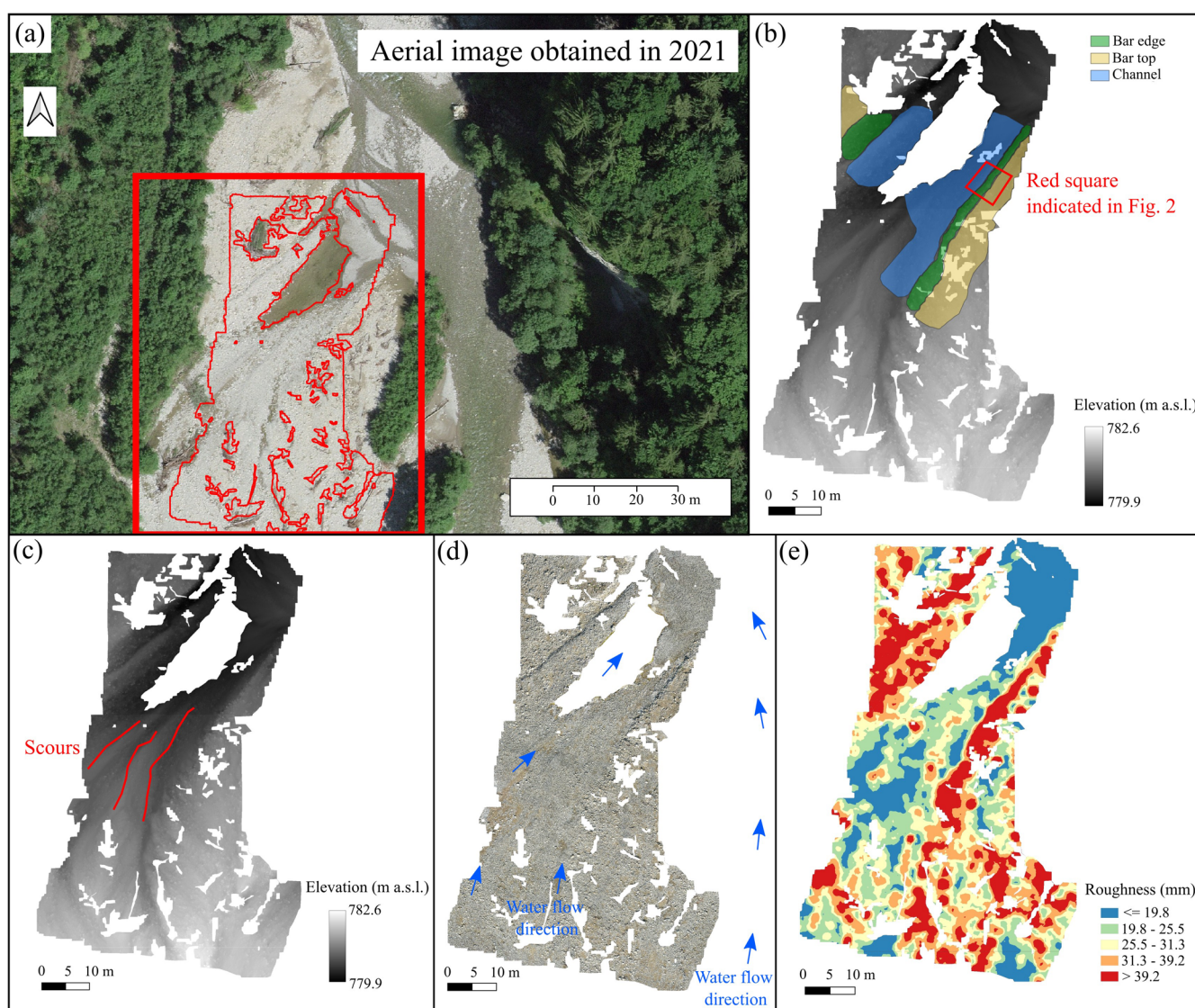


FIGURE 3 Maps of the Sense reach (site A) that was analysed in this work. The areas in white are surfaces that were removed as they hosted vegetation or were covered by wood debris or water bodies. (a) Aerial image obtained in 2021 (© swisstopo, 2024; Mapgeo, 2024). The red square marks the area of interest, and the red line inside the red square delineates the surveyed area displayed in Figures 3b-e. (b) DEM of the surveyed area, showing the bar top, bar edge and the channel. The red square indicates the area that is displayed in Figure 2. (c) DEM of the surveyed area. (d) Orthomosaic of the surveyed area. The indicated flow direction (blue arrows) shows the course of the flow during floods. (e) Roughness map of the surveyed area.

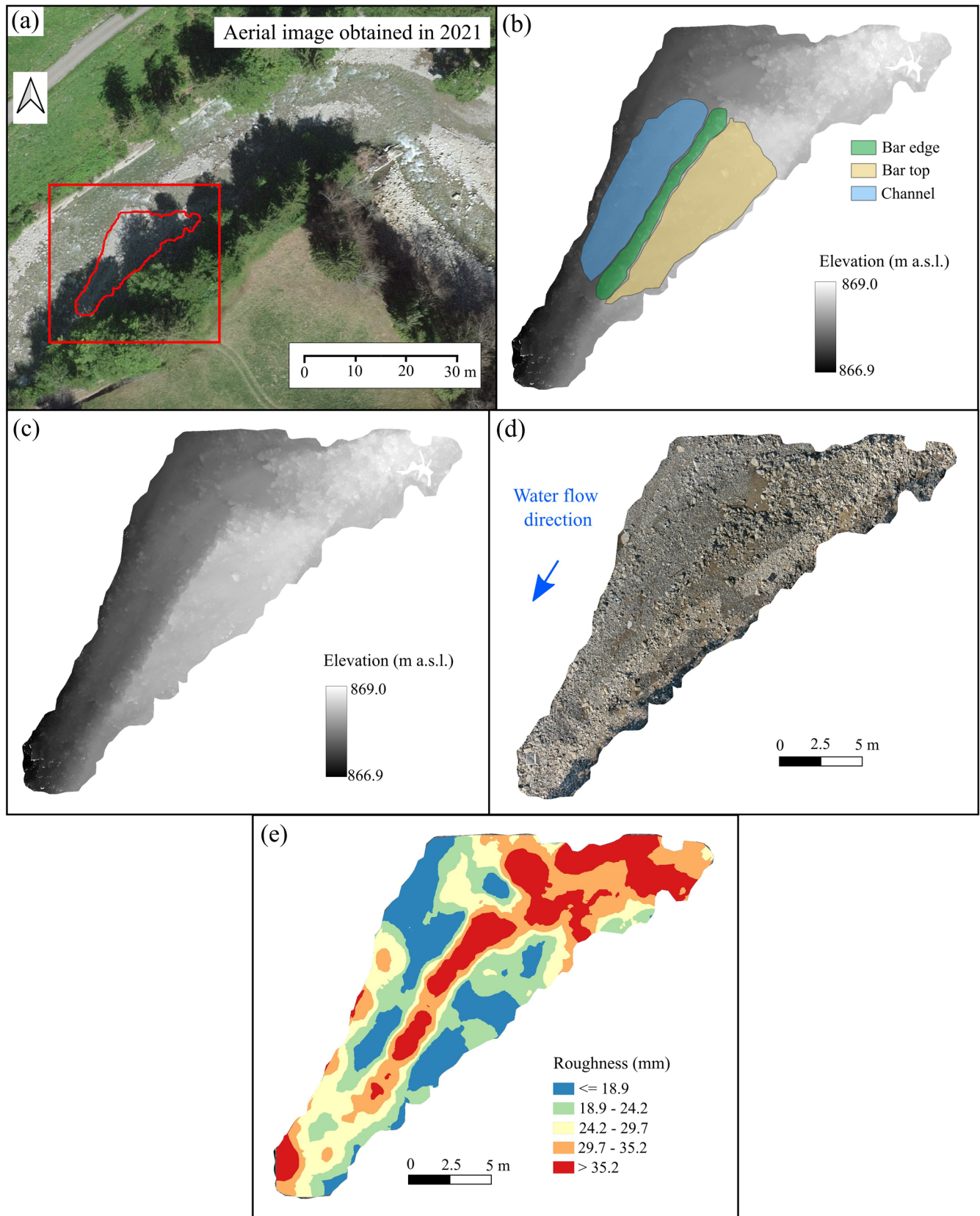


FIGURE 4 Maps of the Kalte Sense reach (site B) that was analysed in this work. The areas in white are surfaces that were removed as they hosted vegetation or were covered by wood debris or water bodies. (a) Aerial image obtained in 2021 (© swisstopo, 2024; Mapgeo, 2024). The red square marks the area of interest, and the red line inside the red square delineates the surveyed area displayed in Figures 4b-e. (b) DEM of the surveyed area, showing the bar top, bar edge and the channel. (c) DEM of the surveyed area. (d) Orthomosaic of the surveyed area. The indicated flow direction (blue arrow) shows the course of the flow during floods. (e) Roughness map of the surveyed area.

4.2 | Roughness and grain size

In general, the roughness values (Equation 1) range from 10 to 40 mm at both sites (Figures 3e, 4e). The largest roughness values ranging from 29 to > 35 mm were measured for the bar edges. Along the channel and on the bar tops, the roughness values are much smaller, ranging between <18 and 29 mm. In addition, the roughness pattern along the channel at Site A is more homogeneous displaying lower variability values than on the bar top where the roughness variability is much higher. In contrast to Site A, the bar top and the channel of Site B have nearly the same roughness values. For both studied reaches, the bar edges have smaller roughness variabilities than the channels and the bar tops despite displaying the largest roughness values (Figures 3e, 4e). Other areas with high roughness values (>35 mm), observed in the northwest and southeast portions of Figure 3e and the northeast part of Figure 4e, are interpreted as riffles.

The cumulative distribution of grain sizes for each of the mapped bed features shows that the material of the bar edges is consistently coarser-grained than the sediment on the bar top and in the channel, at least for the percentile values <D₉₆ (Figure 5). In particular, the largest difference occurs around the D₅₀, where the edges are about twice as coarse than the material of the other two bed features. For the larger percentiles, the differences in the grain sizes are smaller, where the D₈₄ and the D₉₆ values of the edge are about 50% and 25% larger than those of the other bed features, respectively. For any percentile larger than the 98th, the values are indistinguishable between bar top, edge and channel.

4.3 | Bar edge preservation through time

Along the Sense River, multiple coarser-grained bar edges can be detected on the high-resolution orthoimages that were taken during lower flow conditions (see examples in Figure A3 in the Supporting Information; swisstopo, 2024). Using the available aerial images obtained between 2017 and 2023, we identified a large gravel bar without vegetation that displays an erosive edge parallel to the direction of the water flow in the active channel (Figure 6a). In 2017, the bar edge had a higher concentration of coarse-grained material than the bar top. In the following years, the gravel bar remained stable, and vegetation started to grow from 2020 onward, remaining there until at least 2023 (Figures 6c–6e). Despite the stability of the mapped bar,

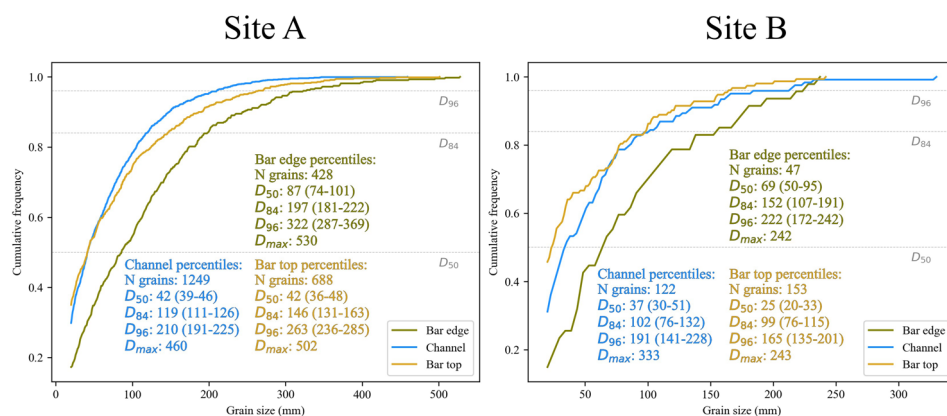
the active channel experienced multiple changes over these six years, with several shifts of its course, including taking a very close position to the bar edges in 2018. Between 2017 and 2019, the hydrological station located approximately 20 km downstream of the preserved bar registered an annual peak discharge of 121 m³ s⁻¹ (FOEN, 2024), which is considered as a lower-discharge flood with a return period of about 2 years (see local setting). In the following years, peak discharges exceeded 150 m³ s⁻¹, with a maximum of 199 m³ s⁻¹ in 2023 (a 10-year peak discharge event), resulting in erosion and reworking of most river bars in the Sense River (e.g. the reach displayed on Figure A4 in the Supporting Information). Only some vegetated bars were preserved after 2020, including the bar in Figure 6. We also observed that on images taken in the years with high-magnitude flood occurrences, the coarse-grained bar edges were more difficult to map compared to those years during which only low-magnitude floods occurred. This is likely due to the reworking of bars and changes in the channel configuration during the high-magnitude floods.

5 | DISCUSSION

5.1 | Lateral lag deposit characteristics, and the stabilization of the river bar through “bar shielding”

Our field-based results demonstrate that the eroded edges of the gravel-cobble bars are composed of coarser material for any grain size percentiles below the 98th compared to the bordering channels and bar tops. Note that for Site A, we assumed the D₉₈ value as not influenced by outliers because the number of observations is higher than 400. In addition, the similarity of grain sizes above the 98th percentile of these bed features shows that they likely originated from the same mixture of material. Accordingly, we interpret that the coarsening observed along the bar edge resulted from the winnowing of the bar edge material during its erosion. We base this interpretation using the results of experiments compiled by Vázquez-Tarrío, Piégay, & Menéndez-Duarte (2020), which illustrate that winnowing during multiple lower-discharge floods leads to a coarsening of the material, thereby forming what they call a riverbed pavement. We infer the same mechanism at work to explain the occurrence of coarse-grained material on the bar edge or lateral lag deposits, which is a process that we also refer to as “bar shielding”. As illustrated in Figure 6, these lag deposits protect and preserve the gravel bars from

FIGURE 5 Cumulative frequency distribution of the grain sizes for the three bed features: bar top, bar edge and channel. The 95% confidence interval of the D₅₀, D₈₄ and D₉₆ were obtained through bootstrapping, and the related values are displayed in brackets. The mapped areas are displayed in Figures 2b and 3b of our study sites.



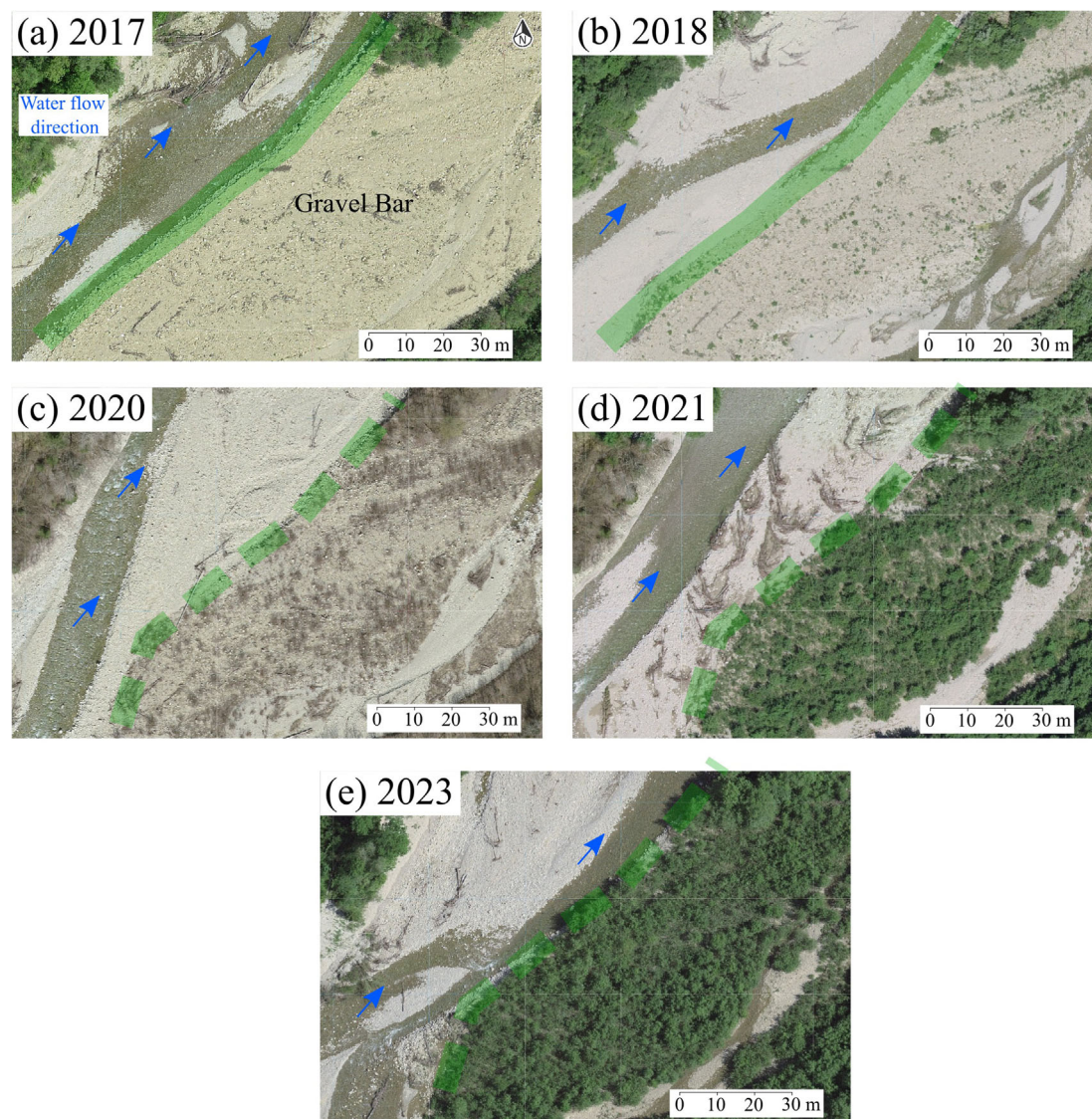


FIGURE 6 Orthoimages showing the temporal preservation of a gravel bar in the Sense River (coordinates: 46.743398° 7.300949°; WGS 84). (a) In the picture obtained in 2017, the indicated gravel bar without vegetation has an original lateral lag deposit marked in green. (b) In 2018, the gravel bar and the lag deposit are still preserved despite the changes in the active channel. (c) In 2020, the preserved gravel bar starts to be covered by vegetation and the original lateral lag deposit was slightly eroded in the upstream part (dashed green line). (d) In 2021, the gravel bar has well-developed vegetation. (e) In 2023, the gravel bar is still preserved even after the occurrence of major flooding events between 2021 and 2023.

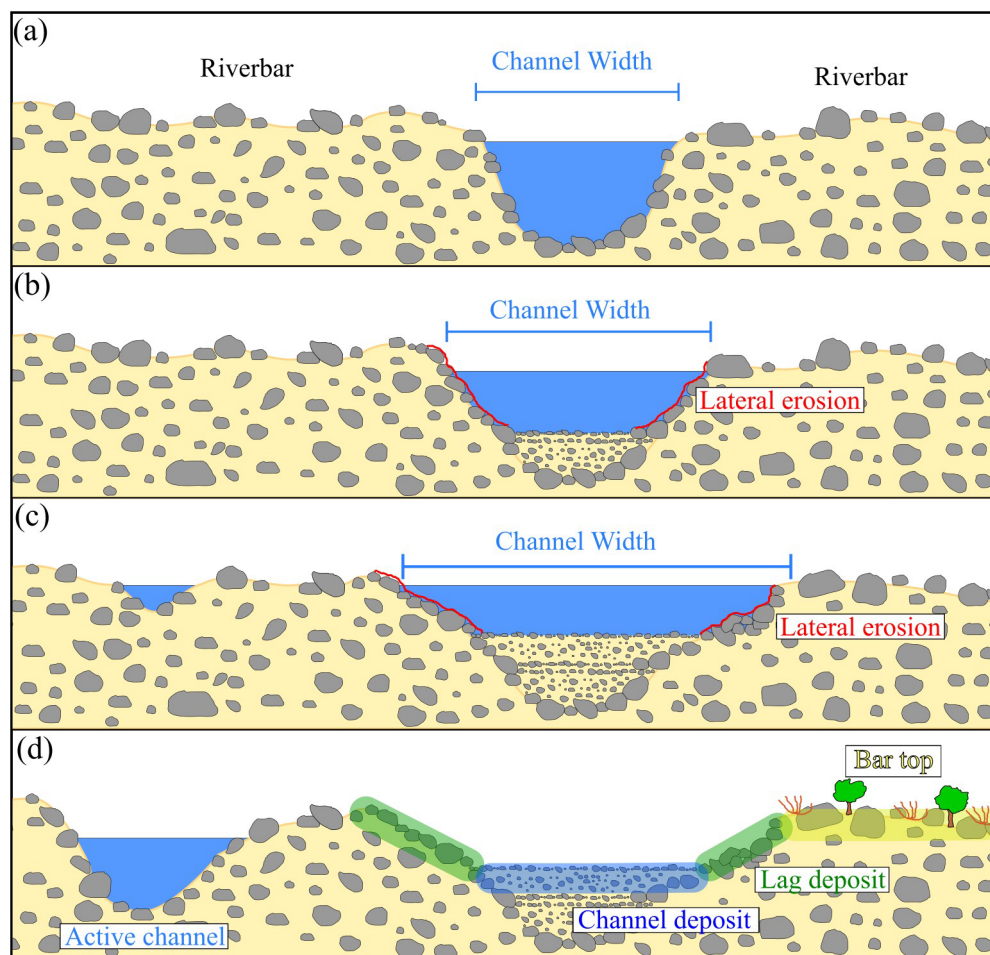
further erosion since their grains are larger than those on the bar top and in the channel. Indeed, because the material is coarser grained in the lateral lag deposits than on the bar top and in the channel, the critical shear stress needed to entrain the material on the bar edge is higher than that required to move particles on the other geomorphic elements. If a flood event induces a shear stress stronger than this critical one, then not only the lag deposit will be eroded but also a large portion of the entire gravel bar. In addition, larger grains in the lateral lag deposit also lead to a higher roughness (Figures 3e and 4e), which amplifies the dissipation of energy on the channel edges. As a result, this increases the turbulences of the flow with the consequence that the shear stress applied by the water along the lateral lag deposit becomes larger. However, this increase appears not to be large enough for the flowing water to erode these sediments during lower-discharge floods. We justify this interpretation using the example displayed in Figure 6, showing that what we interpret as a lateral

lag deposit has been stable during the past 7 years despite the occurrence of multiple lower- and even high-discharge floods.

5.2 | Conceptual model for the formation of a lateral lag deposit and consequence for sediment transport

Here, we propose a conceptual model to explain the formation of a lateral lag deposit (Figure 7). For this model, we consider an initial condition after a high-discharge flood, which resulted in full remobilisation of the riverbed material and which also mixed the grains that were previously deposited farther upstream (Figure 7a). Assuming the occurrence of relatively lower-discharge floods after the first step (Figure 7b), the active channel takes a shallower geometry with finer-grained material deposited in the channel and a larger

FIGURE 7 Conceptual model illustrating the formation of a lateral lag deposit in a cross-section. (a) Initial phase: water flows in a channel over coarse and poorly sorted material after a high-discharge flood that reworked the riverbed and bars. (b) During lower-discharge floods: fine-grained material is deposited on the riverbed and the depth of the channel starts to decrease. At the same time, the channel width increases. This promotes the occurrence of lateral erosion and results in winnowing on the edges of the bars. (c) The aforementioned process continues until the erosive edges of the bar have grains that are sufficiently large to protect the bar from further erosion, thus turning into a stable lateral lag deposit. (d) Final phase: the channel migrates to another position.



width due to lateral erosion of the adjacent bars. A similar process was already described by Eaton, MacKenzie, & Booker (2020), where, during the unstable phase of channel-forming flood events with low sediment supply, riverbank erosion led to the formation of wider and shallower channels. However, in our model, the intensity of the lateral erosion gradually decreases, due to the continuous winnowing of the fine-grained material on the bar edges, leading to a successive coarsening of the sediment (Figure 7c) and thus to a local armouring of the bar edge (Vázquez-Tarrio, Piégay, & Menéndez-Duarte, 2020). Eventually, the channel migrates to another position due to avulsion or new incision during flooding, while the lateral lag deposit is preserved allowing the development of vegetation on the top of the bar (Figure 7d). We consider this as the last step, when roots of the vegetation protect the bars from lateral erosion not only during lower-magnitude floods but possibly also during channel-forming discharge events. Due to the occasional occurrence of flooding events with a high sediment supply, the channel does not transition into the stable phase as described by Eaton, MacKenzie, & Booker (2020). In such a phase, the channel would be expected to adopt a narrower and deeper geometry. In addition, this would be associated with the formation of features that typically form during recurrent low-sediment-supply floods, such as stone lines or pebble clusters, ultimately leading to full riverbed armouring. However, this is not observed in the Sense River. Therefore, the formation and preservation of lateral lag deposits, along with the absence of other features, are linked to the intermittency of floods characterized by both low and high sediment discharge.

In our model, the formation of a lateral lag deposit is an autogenic process that likely influences the sediment budget during lower-discharge flood events. In the absence of lag deposits, lateral erosion of the bars is expected to locally increase the volumes of sediment transported by the river. Thus, the development of these structures can reduce the sediment load during lower-discharge floods, similar to effects observed in fully armoured rivers (e.g. Vázquez-Tarrio, Piégay, & Menéndez-Duarte, 2020). Therefore, if lateral lag deposits are present in a coarse-grained stream, their impact on the occurrence of complete mobilization of the bed material should be considered to improve sediment load predictions during specific lower-discharge floods. We acknowledge that the analysis of only a few gravel bars, as accomplished in this work, provides limited evidence to fully test our conceptual model. Therefore, we recommend that further studies with a larger dataset are still necessary to better understand, and potentially quantify, the threshold conditions required for the complete mobilisation of gravel bars exhibiting lateral lag deposits. Such a dataset could also be used to refine previously published analytical models on bar stability (e.g. Crosato & Mosselman, 2020).

6 | CONCLUSIONS

We investigated the effects of grain size coarsening on river bar edges in the Sense River, Switzerland, and its implications for the stability of gravel-cobble bars devoid of vegetation. Through grain size measurements of mapped bed features, we observed an approximately 50%

increase in the 84th percentile of grain sizes (D_{84}) on eroded bar edges compared to the bar top and channel. These larger grains on the bar edges enhance the stability of the related bar through their effect on the critical shear stress that is required for the bank to be eroded. We termed this phenomenon of gravel bar “shielding”. Additionally, we studied a gravel bar in the Sense River that exhibits a lateral lag deposit and has remained stable for at least six years. Based on these observations, we developed a conceptual model attributing the presence of lateral lag deposits as a key factor contributing to the bar's stability during periods when vegetation was absent on its surface. We suggest that such bar shielding likely occurs in rivers with similar water discharge and sediment transport conditions as in the Sense River, characterized by significant annual peak discharge variations: from lower-discharge floods during which fine-grained material is preferentially transported and during which the riverbed including the lateral lag deposit becomes winnowed, to years with higher-discharge floods when all bed materials are reworked. Consequently, lateral lag deposits are among the first bed features that experience a grain size coarsening due to winnowing, potentially leading to a fully armoured riverbed if the supply of sediment from upstream reaches decreases. Finally, observations of lag deposits in the Sense River provide insights into the mechanisms leading to the stability of river bars made up of poorly sorted sediment and without vegetation. As lateral lag deposits are sedimentological structures of a braided stream that possibly offer, in comparison to other bed features, the largest threshold for being completely reworked, they have the potential to set the condition for the occurrence of complete mobilization of grains along a reach. As already noted by e.g., Wilcock & McArde (1993), Davidson & Eaton (2018) and McKenzie et al. (2018) we still lack experimental and numerical tools to fully understand and compute the complexities of the hydraulic mechanisms including turbulences, energy dissipation and shear stresses operating on channel edges. Yet based on our observations, we suggest that lateral lag deposits exert an important role in the stabilization of channels and may accelerate the re-establishment of riparian forests. Therefore, they should receive more attention in future work on fluvial sedimentology.

AUTHOR CONTRIBUTIONS

Ariel Henrique do Prado: Conceptualization; Formal analysis; Investigation, Methodology, Project administration, Visualization, Writing—original draft, Writing—review and editing. **Cristiano Padalino Galeazzi:** Conceptualization, Visualization, Writing—review and editing. **David Mair:** Investigation, Methodology, Writing—review and editing. **Philippos Garefalakis:** Investigation, Writing—review and editing. **Renato Paes de Almeida:** Conceptualization, Writing—review and editing. **Alexander C. Whittaker:** Funding acquisition, Supervision, Writing—review and editing. **Fritz Schlunegger:** Investigation, Funding acquisition, Project administration, Supervision, Writing—review and editing.

ACKNOWLEDGEMENTS

This project has received funding from the European Union's Horizon 2020 research and innovation programme under the Marie Skłodowska-Curie grant agreement No 860383. This work was also supported by the National Research Foundation of Korea (NRF) grant funded by the Korean government (SRC No. RS-2022-NR070842, G-LAMP No. RS-2023-00301976).

CONFLICT OF INTEREST STATEMENT

The authors declare that they have no known competing financial interests or personal relationships that could have appeared to influence the work reported in this paper.

DATA AVAILABILITY STATEMENT

Data will be made available on request. During the preparation of this work the author(s) used OpenAI/ChatGPT in order to textual corrections. After using this tool/service, the author(s) reviewed and edited the content as needed and take(s) full responsibility for the content of the publication.

ORCID

Ariel do Prado  <https://orcid.org/0000-0003-0135-6239>

David Mair  <https://orcid.org/0000-0002-7018-6416>

REFERENCES

- Aberle, J. & Smart, G. (2003) The influence of roughness structure on flow resistance on steep slopes. *Journal of Hydraulic Research*, 41(3), 259–269. Available from: <https://doi.org/10.1080/00221680309499971>
- Anderson, R.J., Bledsoe, B.P. & Hession, W.C. (2004) Width of streams and rivers in response to vegetation, bank material, and other factors 1. *JAWRA Journal of the American Water Resources Association*, 40(5), 1159–1172. Available from: <https://doi.org/10.1111/j.1752-1688.2004.tb01576.x>
- Ashmore, P. (2013) Morphology and dynamics of braided rivers. In: Schroder, J. & Wohl, E. (Eds.) *Treatise on geomorphology*, Fluvial Geomorphology, Vol. 9. San Diego, CA: Academic Press, pp. 289–312. Available from: <https://doi.org/10.1016/B978-0-12-374739-6.00242-6>
- Bertin, S., Groom, J. & Friedrich, H. (2017) Isolating roughness scales of gravel-bed patches. *Water Resources Research*, 53(8), 6841–6856. Available from: <https://doi.org/10.1002/2016WR020205>
- Bridge, J.S. (2003) *Rivers and floodplains: forms, processes, and sedimentary record*. Malden: Blackwell.
- Bunte, K. & Abt, S.R. (2001) Sampling surface and subsurface particle-size distributions in wadable gravel-and cobble-bed streams for analyses in sediment transport, hydraulics, and streambed monitoring. General Technical Report RMRS-GTR-74. U.S. Department of Agriculture, Forest Service, Rocky Mountain Research Station, Fort Collins, CO, (428 pp.). Available from: <https://doi.org/10.2737/RMRS-GTR-74>
- Carbonneau, P.E. & Dietrich, J.T. (2017) Cost-effective nonmetric photogrammetry from consumer-grade sUAS: implications for direct georeferencing of structure from motion photogrammetry. *Earth Surface Processes and Landforms*, 42(3), 473–486. Available from: <https://doi.org/10.1002/esp.4012>
- Church, M. (1987) River bed gravels: sampling and analysis. In: Thorne, C.-R., Bathurst, J.C. & Hey R.D., (Eds.) *Sediment transport in gravel-bed rivers*. Chichester, U.K.: John Wiley and Sons Ltd, pp. 43–88.
- Church, M. (2006) Bed material transport and the morphology of alluvial river channels. *Annual Review of Earth and Planetary Sciences*, 34(1), 325–354. Available from: <https://doi.org/10.1146/annurev.earth.33.092203.122721>
- Church, M. & Jones, D. (1982) Channel bars in gravel bed rivers. In: Hey, R.-D., Bathurst, J.C. & Thorne, C.R. (Eds.) *Gravel-bed rivers: fluvial processes, engineering, and management*. Chichester: Wiley, pp. 291–338.
- Crosato, A. & Mosselman, E. (2020) An integrated review of river bars for engineering, management and transdisciplinary research. *Water*, 12(2), 596. Available from: <https://doi.org/10.3390/w12020596>
- Davidson, S.L. & Eaton, B.C. (2018) Beyond regime: a stochastic model of floods, bank erosion, and channel migration. *Water Resources Research*, 54(9), 6282–6298. Available from: <https://doi.org/10.1029/2017WR022059>
- do Prado, A.H., Mair, D., Garefalakis, P.E., Schmidt, C.L., Whittaker, A.C., Castelltort, S., et al. (2024) Check dam impact on sediment loads:

- example of the Guérbe River in the Swiss Alps—a catchment scale experiment. *Hydrology and Earth System Sciences*, 28(5), 1173–1190. Available from: <https://doi.org/10.5194/hess-28-1173-2024>
- do Prado, A.H., Mair, D., Garefalakis, P.E., Silveira, B.C., Whittaker, A.C. & Schlunegger, F. (2025) The influence of grain size sorting on the roughness parametrization of gravel riverbeds. *Geomorphology*, 471, 109565. Available from: <https://doi.org/10.1016/j.geomorph.2024.109565>
- Doyle, M.W., Shields, D., Boyd, K.F., Skidmore, P.B. & Dominick, D. (2007) Channel-forming discharge selection in river restoration design. *Journal of Hydraulic Engineering*, 133(7), 831–837. Available from: [https://doi.org/10.1061/\(ASCE\)0733-9429\(2007\)133:7\(831\)](https://doi.org/10.1061/(ASCE)0733-9429(2007)133:7(831))
- Eaton, B.C. (2006) Bank stability analysis for regime models of vegetated gravel bed rivers. *Earth Surface Processes and Landforms: the Journal of the British Geomorphological Research Group*, 31(11), 1438–1444. Available from: <https://doi.org/10.1002/esp.1364>
- Eaton, B.C., MacKenzie, L.G. & Booker, W.H. (2020) Channel stability in steep gravel-cobble streams is controlled by the coarse tail of the bed material distribution. *Earth Surface Processes and Landforms*, 45(14), 3639–3652. Available from: <https://doi.org/10.1002/esp.4994>
- Eltner, A., Kaiser, A., Castillo, C., Rock, G., Neugirg, F. & Abellán, A. (2016) Image-based surface reconstruction in geomorphometry: merits, limits and developments, earth surf. *Dynamis*, 4(2), 359–389. Available from: <https://doi.org/10.5194/esurf-4-359-2016>
- FOEN. (2024) Hydrological data. Federal Office for the Environment, Ittigen, Switzerland. Available from: <https://www.hydrodaten.admin.ch/en/> [09 July 2024].
- Fonstad, M.A., Dietrich, J.T., Courville, B.C., Jensen, J.L. & Carbonneau, P.E. (2013) Topographic structure from motion: a new development in photogrammetric measurement. *Earth Surface Processes and Landforms*, 38(4), 421–430. Available from: <https://doi.org/10.1002/esp.3366>
- Galeazzi, C.P., Almeida, R.P.D. & Do Prado, A.H. (2021) Linking rivers to the rock record: channel patterns and paleocurrent circular variance. *Geology*, 49(11), 1402–1407. Available from: <https://doi.org/10.1130/G49121.1>
- Garefalakis, P., do Prado, A.H., Mair, D., Douillet, G.A., Nyffenegger, F. & Schlunegger, F. (2023) Comparison of three grain size measuring methods applied to coarse-grained gravel deposits. *Sedimentary Geology*, 446, 106340. Available from: <https://doi.org/10.1016/j.sedgeo.2023.106340>
- GEKOBE. (2014) Gewässerentwicklungskonzept Bern. Strategische Planungen nach GSchG/GSchV: Sanierung des Geschiebehaushaltes im Kanton. Schlussbericht: Gewässersystem Sense–Saane–Aare. [Berne river development concept. Strategic planning according to WPA/WPO: mitigation of the bedload budget in the canton. Final report: Sense–Saane–Aare river system]. Bau-, Verkehrs- und Energiedirektion (BVE), Canton Bern; 19.
- Groom, J., Bertin, S. & Friedrich, H. (2018) Evaluation of DEM size and grid spacing for fluvial patch-scale roughness parameterisation. *Geomorphology*, 320, 98–110. Available from: <https://doi.org/10.1016/j.geomorph.2018.08.017>
- Hassan, M.A. (2005) Characteristics of gravel bars in ephemeral streams. *Journal of Sedimentary Research*, 75(1), 29–42. Available from: <https://doi.org/10.2110/jsr.2005.004>
- Hettrich, R., Ruff, A., Tranter, C., Geiger, M., & Köberich, T. (2011) Freiheit für das wilde Wasser, Status und Perspektiven nordalpiner Wildflusslandschaften aus naturschutzfachlicher Sicht—Die WWF-Alpenflusstudie [Freedom for Wild Waters: Status and Perspectives of Northern Alpine Wild River Landscapes from a Nature Conservation Perspective]. WWF: Berlin.
- Ibbeken, H. & Schleyer, R. (1986) Photo-sieving: a method for grain-size analysis of coarse-grained, unconsolidated bedding surfaces. *Earth Surface Processes and Landforms*, 11(1), 59–77. Available from: <https://doi.org/10.1002/esp.3290110108>
- James, M.R., Antoniazza, G., Robson, S. & Lane, S.N. (2020) Mitigating systematic error in topographic models for geomorphic change detection: accuracy, precision and considerations beyond off-nadir imagery. *Earth Surface Processes and Landforms*, 45(10), 2251–2271. Available from: <https://doi.org/10.1002/esp.4878>
- James, M.R. & Robson, S. (2012) Straightforward reconstruction of 3D surfaces and topography with a camera: accuracy and geoscience application. *Journal of Geophysical Research: Earth Surface*, 117(F3), 2011JF002289. Available from: <https://doi.org/10.1029/2011JF002289>
- James, M.R. & Robson, S. (2014) Mitigating systematic error in topographic models derived from UAV and ground-based image networks. *Earth Surface Processes and Landforms*, 39(10), 1413–1420. Available from: <https://doi.org/10.1002/esp.3609>
- Jourdain, C., Claude, N., Tassi, P., Cordier, F. & Antoine, G. (2020) Morphodynamics of alternate bars in the presence of riparian vegetation. *Earth Surface Processes and Landforms*, 45(5), 1100–1122. Available from: <https://doi.org/10.1002/esp.4776>
- MacKenzie, L.G. & Eaton, B.C. (2017) Large grains matter: contrasting bed stability and morphodynamics during two nearly identical experiments. *Earth Surface Processes and Landforms*, 42(8), 1287–1295. Available from: <https://doi.org/10.1002/esp.4122>
- MacKenzie, L.G., Eaton, B.C. & Church, M. (2018) Breaking from the average: why large grains matter in gravel-bed streams. *Earth Surface Processes and Landforms*, 43(15), 3190–3196. Available from: <https://doi.org/10.1002/esp.4465>
- Mair, D., Do Prado, A.H., Garefalakis, P., Lechmann, A., Whittaker, A. & Schlunegger, F. (2022) Grain size of fluvial gravel bars from close-range UAV imagery—uncertainty in segmentation-based data. *Earth Surface Dynamics Discussions*, 2022(5), 1–33. Available from: <https://doi.org/10.5194/esurf-10-953-2022>
- Mao, L., Dell'Agnese, A. & Comiti, F. (2017) Sediment motion and velocity in a glacier-fed stream. *Geomorphology*, 291, 69–79. Available from: <https://doi.org/10.1016/j.geomorph.2016.09.008>
- Mapgeo. (2024) Mapping platform of the Swiss Confederation. Available from: <https://map.geo.admin.ch/> [09 July 2024].
- Millar, R.G. & Quick, M.C. (1993) Effect of bank stability on geometry of gravel rivers. *Journal of Hydraulic Engineering*, 119(12), 1343–1363. Available from: [https://doi.org/10.1061/\(ASCE\)0733-9429\(1993\)119:12\(1343\)](https://doi.org/10.1061/(ASCE)0733-9429(1993)119:12(1343))
- Montgomery, D.R. & Buffington, J.M. (1997) Channel-reach morphology in mountain drainage basins. *Geological Society of America Bulletin*, 109(5), 596–611. Available from: [https://doi.org/10.1130/0016-7606\(1997\)109<0596:CRMIMD>2.3.CO;2](https://doi.org/10.1130/0016-7606(1997)109<0596:CRMIMD>2.3.CO;2)
- Nelson, P.A., Venditti, J.G., Dietrich, W.E., Kirchner, J.W., Ikeda, H., Iseya, F., et al. (2009) Response of bed surface patchiness to reductions in sediment supply. *Journal of Geophysical Research: Earth Surface*, 114(F2), 2008JF001144. Available from: <https://doi.org/10.1029/2008JF001144>
- Noss, C. & Lorke, A. (2016) Roughness, resistance, and dispersion: relationships in small streams. *Water Resources Research*, 52(4), 2802–2821. Available from: <https://doi.org/10.1002/2015WR017449>
- Parker, G. (1978) Self-formed straight rivers with equilibrium banks and mobile bed. Part 2. The gravel river. *Journal of Fluid Mechanics*, 89(1), 127–146. Available from: <https://doi.org/10.1017/S0022112078002505>
- Pizzuto, J.E. (1990) Numerical simulation of gravel river widening. *Water Resources Research*, 26(9), 1971–1980. Available from: <https://doi.org/10.1029/WR026i09p01971>
- QGIS. (2024) QGIS geographic information system. Open source geospatial foundation project. Version 3.28. Available from: <https://qgis.org>
- Recking, A., Frey, P., Paquier, A., Belleudy, P. & Champagne, J.Y. (2008) Feedback between bed load transport and flow resistance in gravel and cobble bed rivers. *Water Resources Research*, 44(5), Available from: <https://doi.org/10.1029/2007WR006219>
- Reid, H.E., Williams, R.D., Brierley, G.J., Coleman, S.E., Lamb, R., Rennie, C.D., et al. (2019) Geomorphological effectiveness of floods to rework gravel bars: insight from hyperscale topography and hydraulic modelling. *Earth Surface Processes and Landforms*, 44(2), 595–613. Available from: <https://doi.org/10.1002/esp.4521>
- Rice, S. & Church, M. (1996) Sampling surficial fluvial gravels; the precision of size distribution percentile sediments. *Journal of Sedimentary*

- Research, 66(3), 654–665. Available from: <https://doi.org/10.2110/jsr.66.654>
- Sambrook Smith, G.H., Best, J.L., Ashworth, P.J., Lane, S.N., Parker, N.O., Lunt, I.A., et al. (2010) Can we distinguish flood frequency and magnitude in the sedimentological record of rivers? *Geology*, 38(7), 579–582. Available from: <https://doi.org/10.1130/g30861.1>
- Shields, A. (1936) Application of similarity principles and turbulence research to bed load movement, SCSC Laboratory, California Institute of Technology, USDA, Pasadena, CA. Available from: <https://authors.library.caltech.edu/records/1hysg-j4j53> (last access: 5 March 2024).
- Smart, G.M., Duncan, M.J. & Walsh, J.M. (2002) Relatively rough flow resistance equations. *Journal of Hydraulic Engineering*, 128(6), 568–578. Available from: [https://doi.org/10.1061/\(ASCE\)0733-9429\(2002\)128:6\(568\)](https://doi.org/10.1061/(ASCE)0733-9429(2002)128:6(568))
- swipos: Swiss Positioning Service. (2024) Available from: <https://www.swisstopo.admin.ch/en/geodata/geoservices/swipos.html>, [last accessed: 12 May 2024].
- swisstopo. (2024) Mapping platform of the Federal Office of Topography, swisstopo. Available from: <https://map.geo.admin.ch> [last accessed: 09 July 2024].
- Tercier, J. & Bieri, P. (1961) 36 Gurnigel. *Geol. Atlas Schweiz* 1:25'000, Karte 1206. Swisstopo.
- Tonolla, D., Geilhausen, M. & Doering, M. (2021) Seven decades of hydrogeomorphological changes in a near-natural (sense river) and a hydropower-regulated (Sarine River) pre-Alpine river floodplain in Western Switzerland. *Earth Surface Processes and Landforms*, 46(1), 252–266. Available from: <https://doi.org/10.1002/esp.5017>
- Vázquez-Tarrió, D., Piégay, H. & Menéndez-Duarte, R. (2020) Textural signatures of sediment supply in gravel-bed rivers: revisiting the Armour ratio. *Earth-Science Reviews*, 207, 103211. Available from: <https://doi.org/10.1016/j.earscirev.2020.103211>
- Venditti, J.G., Nelson, P.A., Bradley, R.W., Hought, D. & Gitto, A.B. (2017) Bedforms, structures, patches, and sediment supply in gravel-bed rivers. In: Tsutsumim, D. & Laronne, J. B. (Eds.) *Gravel-bed rivers: Processes and disasters*. John Wiley & Sons Ltd, pp. 439–466. Available from: <https://doi.org/10.1002/9781118971437.ch16>
- Wilcock, P.R. & McArde, B.W. (1993) Surface-based fractional transport rates: mobilization thresholds and partial transport of a sand-gravel sediment. *Water Resources Research*, 29(4), 1297–1312. Available from: <https://doi.org/10.1029/92WR02748>
- Wolman, M.G. (1954) A method of sampling coarse riverbed material. *Transactions of the American Geophysical Union*, 35, 951. Available from: <https://doi.org/10.1029/TR035i006p00951>
- Wolman, M.G. & Gerson, R. (1978) Relative scales of time and effectiveness of climate in watershed geomorphology. *Earth Surface Processes*, 3(2), 189–208. Available from: <https://doi.org/10.1002/esp.3290030207>

SUPPORTING INFORMATION

Additional supporting information can be found online in the Supporting Information section at the end of this article.

How to cite this article: do Prado, A., Galeazzi, C.P., Mair, D., Garefalakis, P., de Almeida, R.P., Whittaker, A.C. et al. (2025) Gravel bar shielding: A mechanism responsible for bar stability in gravel- and cobble-bedded streams. *Earth Surface Processes and Landforms*, 50(7), e70107. Available from: <https://doi.org/10.1002/esp.70107>